Screened-exchange LDA methods for films and superlattices with applications to the Si(100)2×1 surface and InAs/InSb superlattices

R. Asahi
Department of Physics and Astronomy, Northwestern University, Evanston, Illinois 60208 and Toyota Central R&D Laboratories, Inc., Nagakute, Aichi 480-1192, Japan

W. Mannstadt
Department of Physics and Astronomy, Northwestern University, Evanston, Illinois 60208 and Fachbereich Physik, Philipps-Universitat Marburg, 35032 Marburg, Germany

A. J. Freeman
Department of Physics and Astronomy, and Materials Research Center, Northwestern University, Evanston, Illinois 60208
(Received 22 February 1999; revised manuscript received 11 February 2000)

We have developed efficient screened-exchange local-density approximation (sX-LDA) methods for films and superlattices (FLM/SL) with which to calculate self-consistent electronic structures for both occupied and unoccupied states. Considering nonuniform charge densities and local-field effects in the *z* direction for FLM/SL, we have employed *nonlocal* Thomas-Fermi wave vectors to define the screened-exchange interaction. Three methods, for *bulk*, *superlattice*, and *film*, have been implemented in the full-potential linearized augmented plane wave method. The film sX-LDA method was then applied to the Si(100)2×1 surface. The calculated occupied surface states show very good agreement with experiment. On the other hand, an underestimation of the correction to the unoccupied surface states, by about 0.2 eV, was estimated in comparison with available *GW* calculations. The ionization energy of Si was evaluated with the film geometry to be 5.35 eV by virtue of the quasiparticle corrections, showing good agreement with the experimental value of 5.15 ±0.08 eV. We also present an application of the superlattice sX-LDA method to [001] ordered InAs/InSb heterojunctions and superlattices. Band gaps and band offsets under strained conditions were directly calculated by sX-LDA without any experimental data as input. Slightly larger valence-band offsets than the LDA results, by about 0.08 eV, agree with the consequence of the *GW* calculations, indicating an increase of the potential negativity in the InAs region. This potential change along with the charge redistribution at the interface is found to be crucial to evaluate accurate band gaps of the superlattices.

I. INTRODUCTION

Recent major advances in the quantitative computation of ground-state properties in solids are essentially related to the development of density-functional theory in the local-density approximation (LDA) and the local-spin-density approximation.[1,2] Despite its great success with ground-state properties, as expected this theory does not yield agreement with experimental excitation properties, typically represented by band-gap problems in semiconductors (with usual underestimates by 40–50 %), which originate in the discontinuity of the exchange-correlation potential at integer particle numbers.[3–5]

While the *GW* approximation[6] is a standard approach to obtain more precise quasiparticle states, its heavy computational demands have hampered its application to more complicated and/or larger systems. In addition, determining self-consistent properties within the *GW* approximation is still questionable; recently presented results of fully self-consistent *GW* calculations[7] show a large discrepancy from the observed band gap of Si and the bandwidth of K.

The screened-exchange LDA method (sX-LDA) was first proposed[8] by Bylander and Kleinman in order to obtain a better band gap. Seidl *et al.* showed[9] that the method is actually described in the framework of the generalized Kohn-Sham (GKS) scheme, and that the discontinuity of the exchange-correlation potential is introduced through the nonlocal screened potential. Encouraging results for the band gaps, structural properties, and optical properties were demonstrated for several bulk semiconductor materials.[8–11] The advantages of the sX-LDA over the *GW* calculations are that it is much less computationally demanding, and that it permits the self-consistent determination of ground-state properties.

Excitation properties in films and superlattices (FLM/SL) of semiconductors are related to several important applications: band-gap and band-offset engineering in semiconductor heterostructures, catalytic adsorption processes at semiconductor surfaces, and metal-semiconductor contacts. While simplified basis functions like localized Gaussian basis sets are sometimes employed to reduce the computation time for the *GW* calculations,[12] the greatly reduced computational demands of sX-LDA motivate us to consider the self-consistent determination of the FLM/SL properties.[13]

There is, however, a substantial difference between FLM/SL and the bulk in the treatment by sX-LDA; since spatial nonuniformity in charge densities is essential, at least in the direction perpendicular to the film or superlattice (referred to as the *z* direction), the linear response function is no longer approximated as $\chi(\mathbf{r}-\mathbf{r}')$ which is usually taken for

the bulk sX-LDA. This means that, in contrast to the bulk case, we cannot employ a constant Thomas-Fermi wave vector for FLM/SL.

In this paper, we extend the sX-LDA method for the cases of FLM/SL using a *nonlocal* response function which does not have spatial invariance in the *z* direction, and employ the screened interaction introducing *nonlocal* Thomas-Fermi wave vectors. It is implemented with our full-potential linearized augmented plane wave (FLAPW) method,[14] which has highly accurate representations for both bulk and film geometry. We then present two particular applications in Sec. III, namely, the Si(100)2×1 surface and the InAs/InSb superlattice. The results, including surface states, ionization energy, valence- and conduction-band offsets, and band gaps are compared with available LDA, *GW*, and experimental results to evaluate the accuracy of the methods.

II. THEORETICAL FRAMEWORK

First, we review the sX-LDA method and its application to bulk materials,[8,9] and then present the theoretical framework and its implementation for FLM/SL.

In the sX-LDA, a GKS equation is written invoking perturbation theory as

$$(\hat{h}^{\mathrm{LDA}}+\Delta\hat{v}_{sx})|i\rangle=\epsilon_i^{sx}|i\rangle, \tag{1}$$

where

$$\Delta\hat{v}_{sx}=\hat{v}_{sx}^{\mathrm{NL}}-\hat{v}_{sx}^{L}. \tag{2}$$

Here $\hat{h}^{\mathrm{LDA}}$ is the LDA Hamiltonian, $\hat{v}_{sx}^{\mathrm{NL}}$ the nonlocal screened Fock exchange operator, $\hat{v}_{sx}^{L}$ the corresponding local one, and $|i\rangle$ are the eigenkets of the sX-LDA. The screened Fock exchange operator is given as

$$v_{sx}^{\mathrm{NL}}(\mathbf{r},\mathbf{r}')=-\sum_{j}^{\mathrm{occ}} W(\mathbf{r},\mathbf{r}')\langle\mathbf{r}|j\rangle\langle j|\mathbf{r}'\rangle. \tag{3}$$

Employing the simple Thomas-Fermi screening for $\Delta\hat{v}_{sx}$, we have the screened interaction in the form

$$W(r)=\frac{e^{-k_{\mathrm{TF}}r}}{r}, \tag{4}$$

and the corresponding local potentials,

$$v_{sx}^{L}[\rho(\mathbf{r})]=-2\left(\frac{3}{\pi}\rho(\mathbf{r})\right)^{1/3}F(\gamma), \tag{5}$$

$$F(\gamma)=1-\frac{4}{3}\gamma\arctan\frac{2}{\gamma}-\frac{\gamma^2}{6}\left[1-\left(\frac{\gamma^2}{4}+3\right)\ln\left(1+\frac{4}{\gamma^2}\right)\right]. \tag{6}$$

Here $\gamma=k_{\mathrm{TF}}/q_F$, where k_{TF} is a Thomas-Fermi screening wave vector, and q_F is a Fermi wave vector corresponding to the average density $\bar{\rho}$. It needs to be emphasized that, as discussed in Ref. 8, it is assumed that the *local* screened-exchange density functional has the same dependence on the local density as the LDA exchange functional, so that γ has no dependence on $\rho(\mathbf{r})$ and q_F depends only on $\bar{\rho}$.

Now we consider the case of FLM/SL. The essential difference between FLM/SL and the bulk is that the linear response for the FLM/SL, $\chi(\mathbf{r},\mathbf{r}')$, is spatially nonuniform, necessitating a translationally noninvariant response function in the *z* direction, whereas we used the response function in the form $\chi(\mathbf{r}-\mathbf{r}')$ for the bulk; in other words, we need to include local-field effects in the *z* direction. In the *GW* calculations, the response function and the corresponding screened interaction are directly calculated by the random-phase approximation (RPA). Instead of its heavy evaluation, we employ a rather simple but reasonable nonlocal response function:

$$\chi(\mathbf{r}_1,\mathbf{r}_2)=\chi(r_{12};\rho_{12}), \tag{7}$$

where

$$\rho_{12}=\frac{\rho(z_1)+\rho(z_2)}{2}, \tag{8}$$

i.e., the response function depends on an intermediate density between the planar-averaged densities $\rho(z_1)$ and $\rho(z_2)$ and the distance between the two positions $r_{12}=|\mathbf{r}_1-\mathbf{r}_2|$. Clearly, in a homogeneous system, Eq. (7) is reduced to a response function that depends only on a constant average density over the solid, i.e., the approximation used in sX-LDA for the bulk. Applications of Eq. (7) have been undertaken in calculations for the H_2 molecule[15] and for a surface energy,[16] and give reasonable improvement over the results using the homogeneous form.

Considering the Thomas-Fermi screening function, Eq. (7) yields a screened interaction for FLM/SL as

$$W^{\mathrm{FS}}(r_{12};z_1,z_2)=\frac{e^{-k_{\mathrm{FS}}(z_1,z_2)\,r_{12}}}{r_{12}}, \tag{9}$$

where the *nonlocal* Thomas-Fermi wave vector k_{FS} is defined by

$$[k_{\mathrm{FS}}(z_1,z_2)]^2=\frac{4}{\pi}(3\pi^2\rho_{12})^{1/3}. \tag{10}$$

For a local screened potential, we use Eq. (5) but assume that γ depends on $\rho(z)$, and keep it independent of $\rho(\mathbf{r})$. With this particular choice of screening function, a Fourier component of Eq. (9) is given analytically as

$$\begin{aligned}\tilde{W}^{\mathrm{FS}}(\mathbf{q}_{\mathbf{xy}};z_1,z_2)&=\frac{1}{A}\int d\mathbf{r}_{\mathbf{xy}}\,W^{\mathrm{FS}}(r_{12};z_1,z_2)e^{-i\mathbf{q}_{\mathbf{xy}}\cdot\mathbf{r}_{\mathbf{xy}}}\\&=\frac{2\pi}{A}\int_{d_{12}}^{\infty}dr\,J_0(q_{\mathbf{xy}}\sqrt{r^2-d_{12}^2})e^{-k_{\mathrm{FS}}(z_1,z_2)\,r},\end{aligned} \tag{11}$$

where $\mathbf{q}_{\mathbf{xy}}$ is a two-dimensional wave vector, $d_{12}=|z_1-z_2|$, A is the area of the unit cell, and J_0 is the zeroth order Bessel function.

We evaluate matrix elements $I_{12}=\langle1,\mathbf{k}|v_{sx}^{\mathrm{NL}}|2,\mathbf{k}\rangle$ of the nonlocal screened Fock potential, Eq. (3), for a Bloch state $\mathbf{k}$ for three cases: *bulk*, *superlattice*, and *film*. For the bulk, we follow the implementation and notation given by Massidda *et al.*[17] Each matrix element is given as follows:

(1) *Bulk*. The screened function depends only on $|\mathbf{r}_1-\mathbf{r}_2|$,

$$I_{12}=-\sum_{m,\mathbf{q}}^{\text{occ}}\sum_{\mathbf{G}}\rho^*_{m\mathbf{q}1\mathbf{k}}(\mathbf{G})\rho_{m\mathbf{q}2\mathbf{k}}(\mathbf{G})\tilde{W}(\mathbf{k}-\mathbf{q}+\mathbf{G}). \quad (12)$$

(2) *Superlattice*. The screened function is Eq. (9), but there is a periodicity in the z direction that defines a finite size of the unit cell,

$$I_{12}=-\sum_{m,\mathbf{q}}^{\text{occ}}\sum_{\mathbf{G_{xy}}}\sum_{\mathbf{G_z},\mathbf{G_z'}}\rho^*_{m\mathbf{q}1\mathbf{k}}(\mathbf{G_{xy}},\mathbf{G_z})\rho_{m\mathbf{q}2\mathbf{k}}(\mathbf{G_{xy}},\mathbf{G_z'})\times\tilde{F}^{\text{FS}}(\mathbf{k}-\mathbf{q}+\mathbf{G_{xy}};\mathbf{G_z},\mathbf{G_z'}). \quad (13)$$

(3) *Film*. The screened function is Eq. (9), and there is no periodicity in the z direction:

$$I_{12}=-\sum_{m,\mathbf{q}}^{\text{occ}}\sum_{\mathbf{G_{xy}}}\int_{-\infty}^{\infty}dz\int_{-\infty}^{\infty}dz'\,\rho^*_{m\mathbf{q}1\mathbf{k}}(\mathbf{G_{xy}},z)\times\rho_{m\mathbf{q}2\mathbf{k}}(\mathbf{G_{xy}},z')\tilde{W}^{\text{FS}}(\mathbf{k}-\mathbf{q}+\mathbf{G_{xy}};z,z'). \quad (14)$$

Here the Fourier transforms of the overlap charge density matrices and the screened interactions are defined as

$$\rho_{m\mathbf{q}n\mathbf{k}}(\mathbf{G})=\int d\mathbf{r}\,\psi^*_{m\mathbf{q}}(\mathbf{r})\psi_{n\mathbf{k}}(\mathbf{r})e^{-i(\mathbf{k}-\mathbf{q}+\mathbf{G})\cdot\mathbf{r}}, \quad (15)$$

$$\rho_{m\mathbf{q}n\mathbf{k}}(\mathbf{G_{xy}},z)=\int d\mathbf{r}_{\mathbf{xy}}\,\psi^*_{m\mathbf{q}}(\mathbf{r})\psi_{n\mathbf{k}}(\mathbf{r})e^{-i(\mathbf{k}-\mathbf{q}+\mathbf{G_{xy}})\cdot\mathbf{r}_{\mathbf{xy}}}, \quad (16)$$

$$\tilde{W}(\mathbf{q})=\frac{4\pi}{\Omega(q^2+k_{\text{TF}}^2)}, \quad (17)$$

$$\tilde{F}^{\text{FS}}(\mathbf{k}-\mathbf{q}+\mathbf{G_{xy}})=\sum_N\frac{1}{L}\int_{-L/2}^{L/2}dz\frac{1}{L}\int_{-L/2}^{L/2}dz'\times e^{-i(k_z-q_z)(z-z'-LN)}\tilde{W}^{\text{FS}}\times(\mathbf{k_{xy}}-\mathbf{q_{xy}}+\mathbf{G_{xy}};z,z'+LN), \quad (18)$$

and $\mathbf{G}$ is the reciprocal lattice vector, Ω is the volume of the unit cell, L is the thickness of the unit cell for a supercell geometry, and N are unit cell indices.

We solve the secular equation Eq. (1) self-consistently in a second variational way; the sX-LDA Bloch states $\psi_i(\mathbf{r})=\langle\mathbf{r}|i\rangle$ are expanded in terms of the FLAPW basis set $\psi^0_n(\mathbf{r})$ as

$$\psi_i(\mathbf{r})=\sum_n\psi^0_n(\mathbf{r})\langle n|i\rangle. \quad (19)$$

The representation of our FLAPW method is actually suitable for the film method; the basis function in the vacuum region is given by

$$\phi_{\mathbf{k}+\mathbf{G}}(\mathbf{r})=[A_v(\mathbf{k}+\mathbf{G})u_{\mathbf{k_{xy}}+\mathbf{G_{xy}}}(E_v,z)+B_v(\mathbf{k}+\mathbf{G})\dot{u}_{\mathbf{k_{xy}}+\mathbf{G_{xy}}}(E_v,z)]\exp[i(\mathbf{k}+\mathbf{G})\cdot\mathbf{r_{xy}}], \quad (20)$$

where u and $\dot{u}$ are solutions of the two-dimensional Schrödinger equation given an energy E_v and a position along the z axis, and the coefficients A_v and B_v are determined by the continuity condition at the boundary of the vacuum and the slab surface.[18] Since we do not use periodicity in the z direction, the integral in Eq. (14) is naturally evaluated on real space meshes. Including an extrapolation technique beyond a finite vacuum region, typically 25 a.u., we accurately consider the solution at $z\to\infty$, giving a definite potential without ambiguity due to the constant gauge and, therefore, the work function.

Note that the integral in Eq. (11) is usually converged quickly with a finite range of r. A problem would be found when $q_{\mathbf{xy}}$ and k_{FS} are very small; in practice, however, this case does not contribute to the matrix elements of Eq. (14) since the amplitudes of the corresponding wave functions are negligible.

Starting from the LDA results calculated by the usual FLAPW procedure, we calculate the overlap charge density matrices and construct the matrix elements for the sX-LDA. After diagonalization, the new eigenfunctions obtained are used to update the screened Fock exchange operator and the charge density in the following iteration until the charge densities and eigenfunctions satisfy self-consistency.

III. APPLICATIONS

A. Si(100)2×1 surface

In this section, we report calculations of the Si(100)2×1 surface as an application of the film sX-LDA method. Among extensive experimental and theoretical studies on the 2×1 reconstruction surface of Si(100), there has been a controversial issue: whether the dimers of the surface are asymmetric (buckled) or symmetric (parallel to the surface). Scannning tunneling microscopy images indicated coexistence of the asymmetric and symmetric dimers.[19,20] Low temperature observations, however, showed that the number of asymmetric dimers increases, suggesting that the asymmetric dimer is energetically stable.[20] Several density-functional calculations have also been performed for this system. Some of the results showed that the asymmetric dimers are lower in energy than the symmetric ones by about 0.1 eV/dimer.[21–23] In addition, calculations for the symmetric dimers yield a metallic surface, which is contrary to experimental results.[24–26] However, due to the LDA problem for excitation energies, whether the surface states of the asymmetric dimers lead to a semiconducting or metallic character has remained a question; metallic surfaces were obtained by Krüger and Pollman using the Green-function scattering formalism,[27] and by Zhu, Shima, and Tsukada using the norm-conserving nonlocal pseudopotential,[28] while surface band gaps of 0.1 eV were obtained by the pseudopotential calculations of Ihm, Cohen, and Chadi,[29] and by Dabrowski and Scheffler.[22] Recent GW calculations[30,31] have demonstrated quasiparticle corrections to the LDA surface states, giving well established

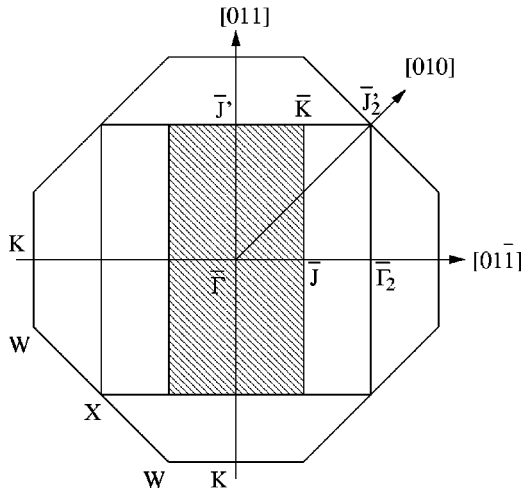

FIG. 1. Surface Brillouin zone of the Si(100)2×1 with the corresponding bulk Brillouin zone. Shaded area shows the first 2×1 surface Brillouin zone.

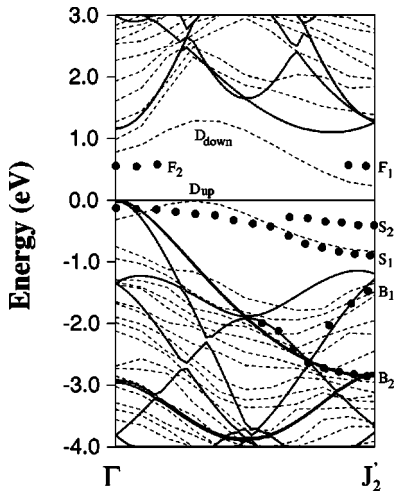

FIG. 2. Self-consistent band structures in the [010] direction for the Si(100)2×1 surface calculated by the film sX-LDA method (dashed lines), and for the bulk Si band structure projected into the 2×1 surface Brillouin zone calculated by the bulk sX-LDA method. Filled circles (labeled *F*, *S*, and *B*) represent the experimental data taken from Ref. 38. The valence-band maximum of bulk Si is set to be zero.

surface band gaps for the asymmetric dimers, while keeping the symmetric dimer surface metallic.[31] Efficient *GW* calculations using model dielectric functions were also performed, showing a difference of about 0.1–0.3 eV in the surface states from the results using the RPA dielectric functions.[31]

As stated in the previous section, the slab geometry of the film method can provide absolute energy levels as we take the potential level far outside the surface to be zero. Work functions of the metal surfaces are thus successfully obtained within the LDA calculations.[18] On the other hand, a difficulty may be found in the case of semiconducting surface states since there is no Fermi surface and the energy levels should include more or less the LDA error. Perdew *et al.* showed[32] that, while the band gap is not correctly evaluated from the Kohn-Sham eigenvalues, the center of the gap relative to the vacuum level is still correct. It is therefore quite interesting to see how accurately we can evaluate the absolute energy levels with self-energy corrections by sX-LDA.

We used a slab containing eight layers of Si, i.e., sixteen Si atoms involved in the unit cell, with hydrogen atoms that saturate the Si dangling bonds at the bottom surface of the slab in order to prevent an interaction between the two surfaces.[31] The atomic positions of the top four layers were allowed to be relaxed and optimized for the 2×1 asymmetric dimer structure using atomic force[33] calculations. The potential level at the vacuum far from the top surface of the slab is chosen to be zero; the vacuum level of the bottom side can be different from zero due to the polarization through the slab. We have also calculated bulk Si using a tetragonal supercell structure whose (001) plane has the same area as the two-dimensional unit cell of Si(100)2×1 to see the folded bulk bands on the surface Brillouin zone (SBZ). The relation between the bulk and surface Brillouin zones is illustrated in Fig. 1.

For the FLAPW-LDA calculations, the exchange-correlation energies were treated using the Hedin-Lundqvist[34] parametrization of the exchange-correlation potential. Cutoffs of the plane wave basis, 9.0 Ry, and of the potential representation, 49 Ry, and an expansion in terms of spherical harmonics with $l \leqslant 8$ inside the muffin-tin spheres were used. The core states were calculated fully relativistically and updated at each iteration, whereas the valence states were treated semirelativistically. The spin-orbit interaction was not included since its effect is very small in Si. Optimized positions were determined within the LDA calculations. For the sX-LDA calculations, we employed cutoff parameters 6.25 Ry for the plane-wave basis, $l \leqslant 4$ for the spherical harmonics, and all occupied and three empty states per atom to achieve convergence of the eigenvalues to within 0.02 eV. Summations over the Brillouin zone for both LDA and sX-LDA self-consistent calculations were done using four special *k* points[35] in the irreducible wedge. We assumed self-consistency of the charge densities and eigenfunctions when the average root-mean-square difference between the input and output charge densities was less than $1 \times 10^{-4}\ e/(\text{a.u.})^3$.

The bulk Si band structure was calculated by the bulk sX-LDA with a tetragonal unit cell. We obtained a fundamental band gap of 1.10 (1.17) eV, an indirect band gap at *X* of 1.26 (1.25) eV, and a valence-band width of 12.78 (12.5 ±0.6) eV, showing very good agreement with experiment[36,37] (values in parentheses). In order to put the bulk band structure together with the film band structure, we used the Si 1*s* core level in the sixth layer from the surface as a reference, which showed good convergence within 0.05 eV between the fifth and the sixth layers. In this way, we have evaluated both the surface band energies and the valence-band maximum (VBM) measured from the vacuum level within the above uncertainty. For convenience, we present all calculated and experimental energies measured from the VBM of bulk Si.

In Fig. 2, we present the band structures of the Si(100)2×1 surface and bulk Si along the [010] direction on the SBZ calculated by the sX-LDA methods, compared with angle-resolved photoemission data.[38] The results for the surface states at symmetry points are summarized in Table I. The occupied surface states (D_{up}) calculated by the film sX-LDA show good agreement with the experimental data in Table I

TABLE I. Calculated surface states (measured from the valence-band maximum in eV) of Si(100)2×1. The results of the *GW* calculations taken from Ref. 31 using the RPA dielectric function (GW-RPA) and the model dielectric functions (Ref. 44) proposed by Hybertsen and Louie (GW-HL), and available experimental data (Expt.) are shown for comparison.

	D_{up}				D_{down}			
	Γ	J	K	J'	Γ	J	K	J'
LDA	−0.35	−0.32	−0.80	−0.92	0.47	0.60	0.09	−0.16
sX-LDA	−0.32	−0.24	−0.77	−0.83	0.78	0.90	0.42	0.23
GW-RPA	−0.15	−0.20	−0.80	−0.85	0.95	1.00	1.10	0.85
GW-HL	−0.30	−0.35	−1.05	−1.05	0.80	0.85	0.95	0.70
Expt.	−0.4, [a] −0.1 [b]	−0.4, [a] −0.1 [b]	−1.0 [a]	−1.0, [a] −0.1 [b]	1.1, [c] 1.2 [d]	1.3 [d]		0.44, [c] 0.55 [d]

[a]Reference 39.
[b]Reference 38.
[c]Reference 25.
[d]Reference 42.

as well as the experimental dispersion S_1 in Fig. 2. A small correction to the LDA D_{up} states, 0.03–0.08 eV, was obtained, as shown in Table I; the LDA calculations already yield good agreement with experiment for the D_{up} states relative to the VBM as seen in other LDA calculations.[28,21] Good agreement between experimentally observed occupied structures B_1 and B_2 and the present folded bulk bands, as shown in Fig. 2, indicates that both structures come from the bulk resonance states: The structure B_2 is coincident with the upper valence bands for bulk Si along the Γ-X direction, and identified as the transition from the bulk valence bands to the free-electron-like final bands.[40] On the other hand, the bulk band along with B_1 comes from the band along the Γ_2-J' direction folded onto the 2×1 domain (see Fig. 1). This directly supports an interpretation where B_1 is explained by the surface Umklapp transition originating from the bulk transition at J'.[38] The rest of the occupied structure S_2 is understood[28,30] to be the surface states associated with the $p(2\times2)$ or $c(4\times2)$ reconstructed surfaces, which are not considered in the present unit cell.

While the FLAPW calculations give a metallic surface as seen in the negative D_{down} state at J', the sX-LDA calculations give a semiconducting surface, which is observed in experiment. We obtained an unoccupied surface band (D_{down}) with the value of 0.78 eV at Γ and the minimum value of 0.23 eV at J_2'. Optical absorption studies[25] showed that indirect and direct transitions take place with thresholds of 0.44 eV at J_2' and 1.1 eV at Γ. In addition, the experimental structure F_1 located around 0.55 eV at J_2' was suggested to be the minimum of the unoccupied dangling-bond bands;[41] with the results of angle-resolved inverse photoemission (IPE), an energy difference of about 0.65 eV between Γ and J_2', the D_{down} state at Γ is estimated to be 1.2 eV. The D_{down} states calculated by sX-LDA are thus concluded to be lower than the experimental values by 0.2–0.4 eV.

In order to analyze the source of this discrepancy with experiment, we compare with the *GW* calculations[31] using the Gaussian orbital LDA (GO-LDA) basis set in Table I. It should be noted that very different results from ours for the D_{down} states at K and J' are mainly due to the discrepancy of the LDA eigenvalues rather than the accuracy of the corrections: measuring from the D_{down} state at Γ, we obtained −0.38 (−0.36) eV at K and −0.63 (−0.55) eV at J' by LDA (sX-LDA), while the GO-LDA calculations (with the *GW* corrections) yield 0.05 (0.15) eV at K and −0.25 (−0.10) eV at J'; our results are, however, closer to the other LDA results,[22,43] −0.37 eV at K, −0.47 eV and −0.57 eV at J', and to the experimental values, −0.67 eV at J' from the IPE results,[41] and −0.66 at J' from the optical absorption studies.[25] On the other hand, focusing on the corrections at Γ where both LDA results agree with each other, we found that the D_{down} states of sX-LDA are lower in energy than those of the *GW* method using the RPA dielectric matrix by about 0.2 eV, but are quantitatively comparable with those of the *GW* method using the model dielectric function (with $\epsilon_\infty = 10.0$) proposed by Hybertsen and Louie.[44] Note that the sX-LDA method has an obvious advantage over the above model dielectric function; the latter needs to calculate or assume the dielectric constant $\epsilon_\infty(\mathbf{r})$ which significantly changes in space at the surface.[30]

The rest of the discrepancy with experiment, which exists in the *GW* calculations as well, probably comes from the insufficient size of the unit cell we considered. Thus an additional correction can be expected by considering a larger unit cell such as $c(4\times2)$, where the two branches for the surface bands, which are observed in experiment, are well described.[28,30] An overestimation of the dimer-dimer interactions in the calculations with a (2×1) unit cell results in a larger dispersion of the surface states and a smaller band gap between two surface states. Zhu *et al.* showed[28] from calculations on the (2×1), $p(2\times2)$, and $c(4\times2)$ unit cells that the band gap between the occupied and unoccupied surface bands is increased by 0.1–0.2 eV with increase of the unit cell from (2×1) to $c(4\times2)$.

The absolute value of the VBM measured from the vacuum level, i.e., the ionization energy, was evaluated by sX-LDA (with a combination of the bulk and film sX-LDA calculations mentioned above) to be 5.35 eV, in good agreement with the experimental value of 5.15±0.08 eV.[45] We also obtained the VBM 4.84 eV from slab and bulk calculations purely within the LDA. Assuming that the center of the band gap at Γ is fixed with respect to the vacuum level, we got a corrected VBM of 5.21 eV after adding one half of the band-gap correction at Γ obtained by the bulk sX-LDA

calculations—confirming numerically the theoretical consequence[32] of Perdew *et al.* for the Kohn-Sham eigenvalues.

In summary, results for the Si(100)2×1 surface calculated by the film sX-LDA method follow. (1) While the occupied surface bands showed good agreement with experiment, there is an underestimation of the quasiparticle correction to the unoccupied surface bands by about 0.2 eV—as estimated in comparison with the *GW* calculations. (2) The sX-LDA method, with a combination of the slab and bulk geometries, yields not only surface states measured from the vacuum level but also accurate ionization energies of the bulk semiconducting materials.

B. InAs/InSb superlattices

Studies on the energy-band alignment in semiconducting heterojunctions and superlattices have received considerable attention particularly for designing optoelectronic devices. Applications of $InAs_{1-x}Sb_x/InAs_{1-y}Sb_y$ alloys and superlattices to infrared detectors and emitters, for example, require a precise band-gap tuning in the order of 10–100 meV.[46–48] Many theoretical approaches to this problem have been undertaken.[49–55] Most of the studies have focused on valence-band offsets (VBO's) based on LDA calculations utilizing the alignment of the average potential[49,50] or the core levels[51–55] at the interface between two different binary semiconductors. To obtain band gaps and conduction-band offsets (CBO's), however, one needs to know the conduction-band levels by fitting parameters with experiment and/or by estimating empirically from the results of each binary constituent.[52,53] In addition, it is usually assumed that the correction to the LDA band gap is independent of stress conditions and/or superlattice periods; its accuracy is not always guaranteed until it is confirmed by experiment or by certain quasiparticle calculations. Quasiparticle calculations based on the *GW* approximation have also been reported for heterojunctions and superlattices.[56–59] In particular, Zhang *et al.* emphasize the importance of the quasiparticle correction to the LDA VBO; they concluded that the *GW* quasiparticle correction to the VBO is 0.12 eV (as much as 30% of the LDA VBO) for GaAs-AlAs heterojunctions, in excellent agreement with experiment.[56] Also, the *GW* method with model dielectric functions has been applied to InAs/GaAs superlattices[59] and AlN/GaN superlattices and ordered alloys.[58]

In this section, we apply our superlattice sX-LDA method to strained $(InAs)_3/(InSb)_3$ [001] superlattices, where we can compare with available LDA calculations[52–54] to see the detailed effects of the methods. We evaluate band offsets using core-level binding energies as references to the alignment at the interface.[52,53] The VBO (ΔE^v) and CBO (ΔE^c) for a heterojunction consist of two contributions:

$$\Delta E^{v,c} = \Delta b + \Delta E_b^{v,c}, \tag{21}$$

where Δb is an interface term that is the difference in energy between two core levels at both sides of the heterojunction, and $\Delta E_b^{v,c}$ is a bulk term that is the difference in energy between two binding energies of the core levels relative to the valence-band maximum or the conduction-band minimum (CBM) in the isolated bulk constituents. As shown previously,[55] the 3×3 superlattice is sufficient to define the interface term Δb since the [001] direction is not much affected by a macroscopic electric field. We evaluate Δb and band gaps for the superlattice by the superlattice sX-LDA method, and examine how the method changes the LDA electronic structure. Since we calculate self-consistent wave functions and charge densities, it is also interesting to see charge transfer induced by sX-LDA; this can be significant at the interface in narrow band-gap materials like InAs and InSb where the FLAPW calculations underestimate the band gaps by 250% and 400%,[60] respectively. The bulk term $\Delta E_b^{v,c}$ depends on ordering directions and strain conditions at the interface considered. Here we are capable of calculating not only ΔE_b^v but also ΔE_b^c directly by the bulk sX-LDA method using a biaxially strained tetragonal unit cell with a lattice parameter a_s that represents the substrate on which the superlattice grows.

TABLE II. Band gaps (in eV) of strained bulk InAs and InSb as well as $(InAs)_3/(InSb)_3$ superlattices calculated by sX-LDA. Corrections to the LDA band gaps (in eV) are also presented in parentheses.

	$a_s=a_{InAs}$	$a_s=a_{av}$	$a_s=a_{InSb}$
InAs	0.46(1.10)	0.14(1.07)	−0.19(1.04)
InSb	0.12(0.98)	0.27(0.99)	0.26(0.98)
$(InAs)_3/(InSb)_3$	−0.02(0.92)	0.09(0.92)	0.04(1.00)

We considered three different lattice parameters, a_{InAs} (6.06 Å), a_{InSb} (6.46 Å), and their average value a_{av} (6.26 Å). Structural optimizations for the bulk and the superlattices were undertaken within the LDA. The In $4d$ states were treated as valence states. Cutoffs of the plane wave basis, 13.0 Ry, and of the potential representation, 64 Ry, were used. The optimized positions were decided by minimizing the total energy and the atomic force on each atom. For the sX-LDA calculations we put In $4d$ states in the core. In both LDA and sX-LDA calculations, summations over the Brillouin zone for bulks and superlattices were done using, respectively, eight and three special k points in the irreducible wedge. As will be discussed later, for an analysis of the charge density, we used the same muffin-tin radius, 2.4 a.u., for In, Sb, and As. The spin-orbit interaction was included in a perturbative approach using self-consistent sX-LDA wave functions and eigenvalues to treat rather large spin-orbit effects in the present systems. Other parameters for the LDA and sX-LDA are the same as in the previous section.

In Table II we show the band gaps of strained bulk InAs and InSb calculated by the bulk sX-LDA. The band gaps of InAs and InSb with their own lattice parameters, 0.46 eV and 0.26 eV,[62] are in excellent agreement with the experimental values of 0.42 eV and 0.24 eV,[61] respectively. The band gap of InAs decreases linearly as the lattice parameter increases from a_{InAs} to a_{InSb}, while that of InSb changes nonlinearly and shows almost the same value for a_{av} and a_{InSb}. This tendency has already been predicted within the LDA, assuming that the quasiparticle correction to the LDA band gap is independent of strain.[52] We show the corrections to our LDA band gaps obtained by the sX-LDA calculations in Table II. The correction of the InSb band gap is almost constant, while that of the InAs band gap is changed by −0.06 eV as the lattice parameter increases—it is small, but about 10% of the

TABLE III. Calculated valence- (VBO) and conduction- (CBO) band offsets (in eV) of strained InAs/InSb heterojunctions. In addition to the present results (sX-LDA), previous LDA results taken from Ref. 52 (WZ) and Ref. 54 (PCF) are also shown for comparison. The CBO's in Ref. 52 are estimated by using experimental band gaps and stress-independent corrections to the LDA.

	$a_s=a_{\mathrm{InAs}}$	$a_s=a_{\mathrm{av}}$	$a_s=a_{\mathrm{InSb}}$
	VBO		
sX-LDA	0.98	0.62	0.34
PCF	0.88	0.54	0.22
WZ	0.91	0.57	0.25
	CBO		
sX-LDA	0.64	0.75	0.79
WZ	0.68	0.68	0.68

change in the band gap itself, -0.65 eV. These results suggest that the assumption of independence of the band-gap correction to pressure for the bulk binaries is good overall as long as we are concerned about a small change in the band gap induced by stress. We note that the band gap of InSb with the InAs lattice parameter was calculated to be 0.12 eV, which shows the largest difference from the result of 0.19 eV given in Ref. 52. This is not from a difference in the quasiparticle corrections to LDA but from the difference in the LDA band gaps themselves, possibly because of the slightly different unit cell optimized by the total energy. The band gap of InSb with the InAs lattice parameter is quite sensitive to the size of the unit cell; in fact, we observed that a decrease of c/a by 0.6% from the optimized value increases the band gap by 0.06 eV with a very small increase (by 2 meV) of the total energy.

The calculated band offsets are shown in Table III. While two previous LDA results[52,54] for the VBO agree with each other to within 0.03 eV, a systematic increase of the VBO by 0.05–0.12 eV is obtained by the sX-LDA calculations. This correction agrees with the quasiparticle correction to the VBO for the unstrained InAs/InSb heterojunction, 0.08 eV, obtained by *GW* calculations,[57] indicating that our method describes reasonable quasiparticle states and VBO's. The CBO's of the sX-LDA are also larger than the LDA results obtained by Wei and Zunger[52] corresponding to the difference in the VBO, except for the InAs substrate, where their smaller VBO cancels the larger band gap, as mentioned above.

We present in Table II the calculated band gaps at Γ of [001] ordered $(\mathrm{InAs})_3/(\mathrm{InSb})_3$ superlattices. Small band gaps, within ± 0.1 eV, for all three substrates were obtained, although we might expect larger negative ones due to the large VBO. Similar small band gaps were also reported for 1×1 superlattices.[53] The period of these superlattices is actually too short to establish bulklike valence and conduction bands, due to their strong hybridization at the interface, in contrast with the localized core levels that are quickly converged with respect to the period of the superlattices. The corrections to the LDA band gaps in Table II, however, suggest that it is not easy to estimate accurate band gaps of the superlattices from the LDA results and the corrections for the bulk binaries. For example, while the correction to the superlattice band gap with the InSb substrate may be estimated by the average of the corrections for the two binary constituents as used in Ref. 53, this is not the case for the InAs and average substrates. The different corrections are considered to result mainly from a change of the wave-function character and localization at the VBM, and from neglecting many-body effects on the potential at the interface—as will be discussed below.

In Table IV, we show crystal-field splittings at the VBM, which are defined by the difference in energy between the doubly degenerate state Γ_{5v} and the state Γ_{4v}, calculated by sX-LDA and LDA. The values for the 1×1 superlattice are taken from Ref. 53. The results show a decrease of the crystal-field splitting as the substrate lattice parameter increases, and a significant interchange of the wave-function character at the VBM from Γ_{5v} to Γ_{4v} for the InSb substrate. The Γ_{5v} and Γ_{4v} states are found to be highly localized at the interface; the former is on the Sb site and the latter is on the As site. Thus, the above trend suggests that the energy bands of the InAs side shift upward relative to those of the

TABLE IV. Calculated crystal-field splittings at the valence-band maximum (Δ_{CF} in eV) and localizations of the VBM (R_v) and the CBM (R_c) densities, calculated by sX-LDA and LDA (in parentheses). A positive crystal-field splitting means the doubly degenerate Γ_{5v} state is located above the Γ_{4v} state. Localization is defined by the ratio of the angular decomposition (the *p* state for R_v and the *s* state for R_c) of the muffin-tin charge density on the As site to that on the Sb site at the interface of $(\mathrm{InAs})_3/(\mathrm{InSb})_3$ superlattices.

	$a_s=a_{\mathrm{InAs}}$	$a_s=a_{\mathrm{av}}$	$a_s=a_{\mathrm{InSb}}$
	Δ_{CF}		
$(\mathrm{InAs})_1/(\mathrm{InSb})_1$	(0.46 [a])	(0.06 [a])	(-0.25 [a])
$(\mathrm{InAs})_3/(\mathrm{InSb})_3$	0.74(0.57)	0.24(0.11)	$-0.08(-0.15)$
InAs	0.00(0.00)	$-0.35(-0.33)$	$-0.62(-0.57)$
InSb	0.97(0.90)	0.41(0.38)	0.00(0.00)
	R_v		
$(\mathrm{InAs})_3/(\mathrm{InSb})_3$	0.35(0.45)	0.42(0.53)	1.33(1.54)
	R_c		
$(\mathrm{InAs})_3/(\mathrm{InSb})_3$	1.32(1.19)	1.16(1.04)	1.00(0.88)

[a]Reference 53.

InSb side as the lattice parameter increases. From a comparison between two periods of the superlattices in Table IV, we found that the longer period gives a greater shift of the energy bands of the InAs side downward relative to those of the InSb side—recovering the VBO in the heterojunction. To show the localization of the VBM and CBM states in more detail, we present in Table IV the ratio of the angular decomposition of the muffin-tin charge density on the As site to that on the Sb site at the interface. We took the dominant components, the *p*-like and *s*-like states for the VBM and the CBM, respectively. Note that the *s*-like component is also large on the In sites and gives a qualitatively similar trend as listed in Table IV; however, in this case more localization of the CBM in the InSb region is observed for the InSb substrate. The localization at the VBM is changed significantly from the Sb side to the As side when the interchange of the wave-function character at the VBM occurs, as mentioned above. On the other hand, the localization of the CBM is changed from the InAs side to the InSb side as the lattice parameter increases.

From these results, we depict the band alignments of the short-period superlattice as shown in Fig. 3. Note that Fig. 3 is not a rigorous way to express the real situation since the VBM and CBM in superlattices cannot be resolved in real space, but rather an intuitive way, where the trend of the atomic-scale localization in Table IV is consistently described. Also, we put the band alignments of the heterojunctions in Fig. 3, although we cannot determine the relative energy positions of the superlattice and the heterojunction. The trend of the band alignment for the superlattices with respect to the lattice parameter is similar to that of the VBO for the heterojunctions. Both trends result mainly from the change in the crystal-field splitting of the VBM. From Fig. 3, we expect a spatially indirect gap for all three substrates; however, there is also the possibility of obtaining a spatially direct gap in the InSb region with a lattice parameter between a_{av} and a_{InSb}.

Comparing with the LDA results in Table IV, we found that the sX-LDA results give an increase of the crystal-field splitting, and, correspondingly, more charge on the InSb side for the VBM and on the InAs side for the CBM. These changes are considered to come from a many-body correction to the LDA potential,[56] which enhances an ionic bonding structure and leads to a more negative potential in InAs. We can see this effect more clearly using Fig. 3: a shift of the InAs bands downward relative to the InSb bands leads to more weight coming from InSb for the VBM and to more weight coming from InAs for the CBM. Furthermore, the reason why the band-gap correction for the InSb substrate in Table II is larger than that for the other substrates can be understood as follows: in the case of a spatially indirect minimum gap with the VBM localized in the InSb (InAs) region, the above relative shift of the potential by the sX-LDA reduces (increases) the band-gap correction estimated from the corrections for the binary constituents, while the gap of the superlattice with a spatially direct minimum gap does not depend so much on the potential shift. Thus the band-gap correction for the InAs and averaged substrates is smaller than that of each binary constituent.

In summary, the sX-LDA scheme, with a combination of the bulk and superlattice methods, yields accurate valence- and conduction-band offsets in heterojunctions without knowing any experimental values, as confirmed by comparing with previous LDA calculations and the *GW* quasiparticle corrections. Also, the superlattice sX-LDA method provides direct calculations of the band gaps in superlattices. The many-body corrections by the sX-LDA modify the LDA potential so that the ionic feature at the interface is more conspicuous, causing a larger VBO and crystal-field splitting. These effects are sometimes crucial to evaluate electronic structures of narrow band-gap superlattices.

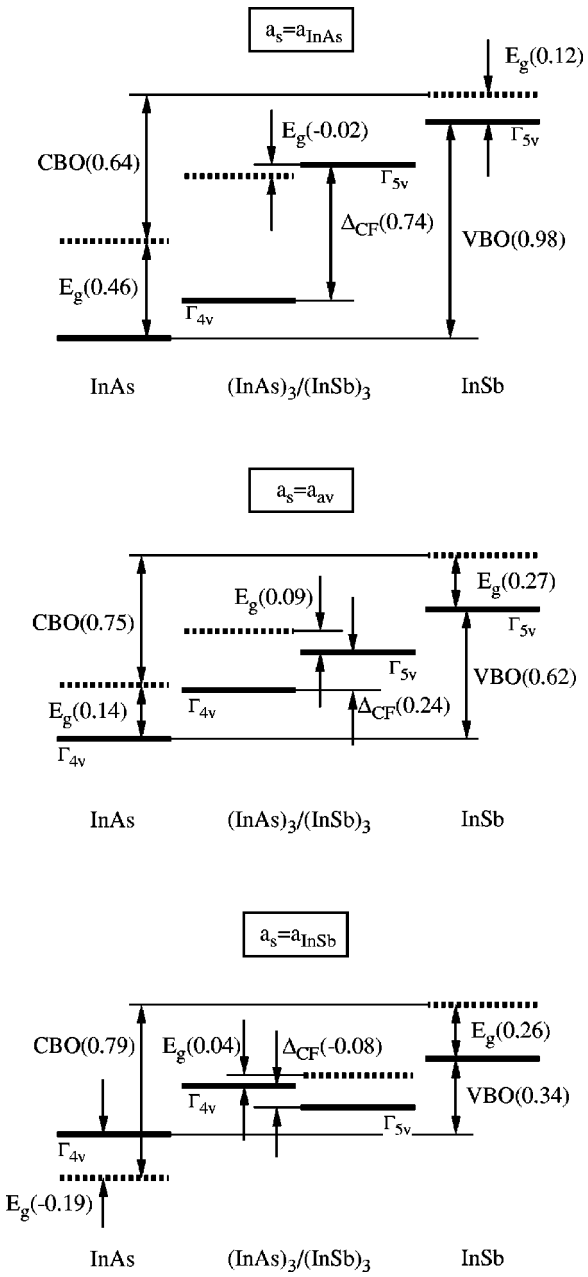

FIG. 3. Schematic band alignment of strained $(InAs)_3/(InSb)_3$ superlattices and InAs/InSb heterostructures. Thick solid and dotted lines show valence-band maxima and conduction-band minima, respectively. For the superlattice, the left half represents the $(InAs)_3$ region and the right half represents the $(InSb)_3$ region; each band is indicated only in a more localized region. Calculated band gaps (E_g), valence-band offsets (VBO's), conduction-band offsets (CBO's), and crystal-field splittings (Δ_{CF}) are presented in parentheses (in eV).

IV. CONCLUSION

We have developed sX-LDA methods to apply to FLM/SL by introducing the film and superlattice methods in addition to the traditional bulk approach. The main idea used to extend sX-LDA to FLM/SL is to consider local-field effects in the z direction. These methods have been successfully implemented with the FLAPW method, which is capable of treating both two-dimensional slab and bulk geometries. Two applications presented here, the Si(100) 2×1 surface and InAs/InSb superlattices, have demonstrated that the methods yield good quasiparticle corrections in comparison with GW calculations. The beneficial features of the present method—no parameters required, less computationally demanding, and self-consistent evaluation of the properties—provide a wide range of applicability. In particular, we saw significant corrections to the electronic structure by the sX-LDA even when LDA calculations gave an erroneous metallic band structure in semiconducting materials. On the other hand, a certain limitation exists in the present approach. This was seen in the slight underestimation of the correction to the Si surface states. To improve the accuracy, more rigorous correlation or screening effects, e.g., full consideration of the local-field effects or going beyond the Thomas-Fermi description, may be required.

ACKNOWLEDGMENTS

We thank S. Picozzi for useful information and discussions about the FLAPW calculations for InAs/InSb superlattices. This work was supported by the NSF (through the Materials Research Center of Northwestern University).

[1] P. Hohenberg and W. Kohn, Phys. Rev. **136**, B864 (1964).
[2] W. Kohn and L. J. Sham, Phys. Rev. **140**, A1133 (1965).
[3] S. B. Trickey, F. R. Green, Jr., and F. W. Averill, Phys. Rev. B **8**, 4822 (1973).
[4] J. P. Perdew and M. Levy, Phys. Rev. Lett. **51**, 1884 (1983).
[5] L. J. Sham and M. Schlüter, Phys. Rev. Lett. **51**, 1888 (1983); Phys. Rev. B **32**, 3883 (1985).
[6] L. Hedin, Phys. Rev. **139**, A796 (1965).
[7] W.-D. Schöne and A. G. Eguiluz, Phys. Rev. Lett. **81**, 1662 (1998).
[8] B. M. Bylander and L. Kleinman, Phys. Rev. B **41**, 7868 (1990).
[9] A. Seidl, A. Görling, P. Vogl, J. A. Majewski, and M. Levy, Phys. Rev. B **53**, 3764 (1996).
[10] R. Asahi, W. Mannstadt, and A. J. Freeman, Phys. Rev. B **59**, 7486 (1999).
[11] W. Wolf, E. Wimmer, S. Massidda, M. Posternak, and C. B. Geller, Bull. Am. Phys. Soc. **43** (1), 797 (1998).
[12] M. Rohlfing, P. Krüger, and J. Pollmann, Phys. Rev. B **57**, 6485 (1998).
[13] R. Asahi, W. Mannstadt, and A. J. Freeman, Bull. Am. Phys. Soc. **44** (1), 1668 (1999).
[14] E. Wimmer, H. Krakauer, M. Weinert, and A. J. Freeman, Phys. Rev. B **24**, 864 (1981), and references therein; M. Weinert, E. Wimmer, and A. J. Freeman, *ibid.* **26**, 4571 (1982); H. J. F. Jansen and A. J. Freeman, *ibid.* **30**, 561 (1984).
[15] S. Chakravarty, J. H. Rose, D. Wood, and N. W. Ashcroft, Phys. Rev. B **24**, 1624 (1981).
[16] J. H. Rose and J. F. Dobson, Solid State Commun. **37**, 91 (1981).
[17] S. Massidda, M. Posternak, and A. Baldereschi, Phys. Rev. B **48**, 5058 (1993).
[18] H. Krakauer, M. Posternak, and A. J. Freeman, Phys. Rev. B **19**, 1706 (1979); M. Posternak, H. Krakauer, A. J. Freeman, and D. D. Koelling, *ibid.* **21**, 5601 (1980).
[19] R. J. Hamers, R. M. Tromp, and J. E. Demuth, Phys. Rev. B **34**, 5343 (1986).
[20] R. A. Wolkow, Phys. Rev. Lett. **68**, 2636 (1992).
[21] P. Kruger and J. Pollmann, Phys. Rev. B **47**, 1898 (1993).
[22] J. Dabrowski and M. Scheffler, Appl. Surf. Sci. **56**, 15 (1992).
[23] N. Roberts and R. J. Needs, Surf. Sci. **236**, 112 (1990).
[24] W. Mönch, P. Koke, and S. Krueger, J. Vac. Sci. Technol. **19**, 313 (1981).
[25] Y. J. Chabal, S. B. Christman, E. E. Chaban, and M. T. Yin, J. Vac. Sci. Technol. A **1**, 1241 (1983).
[26] R. J. Hamers and U. K. Köhler, J. Vac. Sci. Technol. A **7**, 2854 (1989).
[27] P. Krüger and J. Pollmann, Phys. Rev. B **38**, 10 578 (1988).
[28] Z. Zhu, N. Shima, and M. Tsukada, Phys. Rev. B **40**, 11 868 (1989).
[29] J. Ihm, M. L. Cohen, and D. J. Chadi, Phys. Rev. B **21**, 4592 (1980).
[30] J. E. Northrup, Phys. Rev. B **47**, 10 032 (1993).
[31] M. Rohlfing, P. Krüger, and J. Pollmann, Phys. Rev. B **52**, 1905 (1995); **52**, 13 753 (1995).
[32] J. P. Perdew, R. G. Parr, M. Levy, and J. L. Balduz, Phys. Rev. Lett. **49**, 1691 (1982).
[33] R. Yu, D. Singh, and H. Krakauer, Phys. Rev. B **45**, 8671 (1991).
[34] L. Hedin and B. I. Lundqvist, J. Phys. C **4**, 2064 (1971).
[35] H. J. Monkhorst and J. D. Pack, Phys. Rev. B **13**, 5188 (1976).
[36] *Numerical Data and Functional Relationships in Science and Technology*, edited by K.-H. Hellwege, O. Madelung, M. Schulz, and H. Weiss, Landolt-Börnstein, New Series, Group III, Vol. 17, Pt. a (Springer, Berlin, 1982).
[37] J. E. Ortega and F. J. Himpsel, Phys. Rev. B **47**, 2130 (1993).
[38] L. S. O. Johansson, R. I. G. Uhrberg, P. Mårtensson, and G. V. Hansson, Phys. Rev. B **42**, 1305 (1990).
[39] R. I. G. Uhrberg, G. V. Hansson, J. M. Nicholls, and S. A. Flodström, Phys. Rev. B **24**, 4684 (1981).
[40] T.-C. Chiang, R. Ludeke, M. Aono, and G. Landgren, Phys. Rev. B **27**, 4770 (1983).
[41] L. S. O. Johansson and B. Reihl, Surf. Sci. **269/270**, 810 (1992).
[42] Estimated from Refs. 41 and 38 assuming that the structure F at J_2' in Ref. 38 corresponds to the bottom of the structure S_2' in Ref. 41.
[43] K. Kobayashi, Y. Morikawa, K. Terakura, and S. Blügel, Phys. Rev. B **45**, 3469 (1992).
[44] M. S. Hybertsen and S. G. Louie, Phys. Rev. B **37**, 2733 (1988).
[45] F. G. Allen and G. W. Gobeli, Phys. Rev. **127**, 150 (1962).
[46] S. R. Kurtz and R. M. Biefeld, Phys. Rev. B **44**, 1143 (1991).
[47] S. R. Kurtz, R. M. Biefeld, L. R. Dawson, K. C. Baucom, and A. J. Howard, Appl. Phys. Lett. **64**, 812 (1994).
[48] Y.-H. Zhang, R. H. Miles, and D. H. Chow, IEEE J. Sel. Top. Quantum Electron. **1**, 749 (1995).

[49] M. Cardona and N. E. Christensen, Phys. Rev. B **35**, 6182 (1987).
[50] C. G. Van de Walle, Phys. Rev. B **39**, 1871 (1989).
[51] S.-H. Wei and A. Zunger, Appl. Phys. Lett. **58**, 2684 (1991).
[52] S.-H. Wei and A. Zunger, Phys. Rev. B **52**, 12 039 (1995).
[53] S. Picozzi, A. Continenza, and A. J. Freeman, Phys. Rev. B **52**, 5247 (1995).
[54] S. Picozzi, A. Continenza, and A. J. Freeman, Phys. Rev. B **53**, 10 852 (1996).
[55] S. Picozzi, A. Continenza, and A. J. Freeman, Phys. Rev. B **55**, 13 080 (1997).
[56] S. B. Zhang, M. L. Cohen, S. G. Louie, D. Tománek, and M. S. Hybertsen, Phys. Rev. B **41**, 10 058 (1990).
[57] X. Zhu and S. G. Louie, Phys. Rev. B **43**, 14 142 (1991).
[58] A. Rubio, J. L. Corkill, and M. L. Cohen, Phys. Rev. B **49**, 1952 (1994).
[59] R. Padjen and D. Paquet, Phys. Rev. B **43**, 4915 (1991).
[60] S. Massidda, A. Continenza, A. J. Freeman, T. M. de Pascale, F. Meloni, and M. Serra, Phys. Rev. B **41**, 12 079 (1990).
[61] W. A. Harrison, *Electronic Structure and the Properties of Solids* (Freeman, San Francisco, 1980).
[62] The smaller band gap of InSb in Ref. 10 came partly from the difference between cubic and tetragonal unit cells and partly from the treatment of the In 4*d* semicore states, which were put in the second panel of the valence bands in Ref. 10, while being treated as core states in the present calculations. This discrepancy (8% of the quasiparticle correction), however, does not change the qualitative trends in the present results.